Polymer 49 (2008) 5474–5481

Contents lists available at ScienceDirect

Polymer

journal homepage: www.elsevier.com/locate/polymer

Sustained release properties of arborescent polystyrene-*graft*-poly(2-vinylpyridine) copolymers

Gabriel N. Njikang, Mario Gauthier*, Jieming Li

Department of Chemistry, Institute for Polymer Research, University of Waterloo, 200 University Avenue West, Waterloo, Ontario N2L 3G1, Canada

ARTICLE INFO

Article history:
Received 1 August 2008
Received in revised form 3 October 2008
Accepted 6 October 2008
Available online 14 October 2008

Keywords:
Arborescent polymers
Dendrigraft polymers
Drug release

ABSTRACT

The release kinetics of small molecules from dendritic graft copolymer micelles incorporating an arborescent polystyrene (PS) core and a poly(2-vinylpyridine) (P2VP) shell were investigated in dilute HCl solutions by fluorescence and UV spectroscopies. The redistribution of pyrene and perylene among arborescent micelles was studied by the fluorescence resonance energy transfer (FRET) technique, and was characterized by an initial burst in exchange followed by gradual equilibration of the probes. Fluorescence quenching experiments demonstrated that the diffusion coefficient of pyrene increased for copolymer micelles of higher generations, suggesting a more porous shell structure for the higher generation arborescent PS-*g*-P2VP copolymers. *In vitro* release tests for indomethacin and lidocaine monitored by UV spectroscopy showed that sustained release characteristics were achieved, the release rate being higher for lidocaine due to its higher water solubility at low pH. The release rate of indomethacin increased for lower generation micelles and for higher micelle loadings, in agreement with a diffusion-controlled release mechanism. An increasing fraction of the indomethacin molecules loaded in the micelles remained trapped for higher generation copolymers. The diffusion coefficient and the release rate of indomethacin were calculated by fitting the solution of Fick's second law of diffusion to the experimental data. While the initial release rate decreased for higher generations, the trends observed for the diffusion coefficients were similar to those determined for pyrene in the fluorescence quenching experiments. This result is again consistent with a more diffuse shell structure for higher generation micelles, possibly due to the enhanced electrostatic repulsions between the charged P2VP chains.

1. Introduction

Polymeric micelles have attracted much attention as controlled release devices, particularly for hydrophobic compounds [1–5]. Biocompatible amphiphilic block copolymers, for example, have been investigated for the controlled release of hydrophobic drugs [5]. These micelles are able to solubilize large quantities of active molecules in their hydrophobic core and to gradually release them in a controllable manner. The use of unimolecular micelles as controlled release vehicles is particularly interesting because of their stable, covalently bonded structure [6,7]. For example, indomethacin molecules were encapsulated in unimolecular micelles incorporating a hydrophobic dendrimer core and a hydrophilic shell [8]. In contrast to the rapid equilibration time (4 h) observed when free indomethacin dissolved in phosphate buffer solution was dialyzed against phosphate buffer solution at 37 °C, equilibration was observed only after about 25 h for the encapsulated molecules.

Arborescent polystyrene-*graft*-poly(2-vinylpyridine) (PS-*g*-P2VP) copolymers are dendritic unimolecular micelles composed of a glassy branched PS core grafted with hydrophilic P2VP chains forming a shell (Fig. 1). The PS core is synthesized from polymeric chains according to a generation-based scheme consisting of functionalization and grafting reaction cycles. Grafting PS chains ($M_w \approx 5000$) onto a randomly functionalized linear PS backbone ($M_w \approx 5000$) yields a comb-branched or generation *G*0 PS core. Subsequent functionalization and grafting reactions lead to higher generation (*G*1, *G*2…) PS cores with a dendritic architecture. Coupling living P2VP chains ($M_w \approx 5000$) with PS cores randomly functionalized with grafting sites yields amphiphilic macromolecules expected to encapsulate and slowly release hydrophobic molecules in a sustained fashion, in analogy to block copolymer micelles. The advantages of the arborescent micelles relatively to block copolymer micelles include enhanced structural stability

* Corresponding author. Tel.:+1 519 888 4567; fax: +1 519 746 0435.
E-mail address: gauthier@uwaterloo.ca (M. Gauthier).

0032-3861/$ – see front matter © 2008 Elsevier Ltd. All rights reserved.
doi:10.1016/j.polymer.2008.10.002

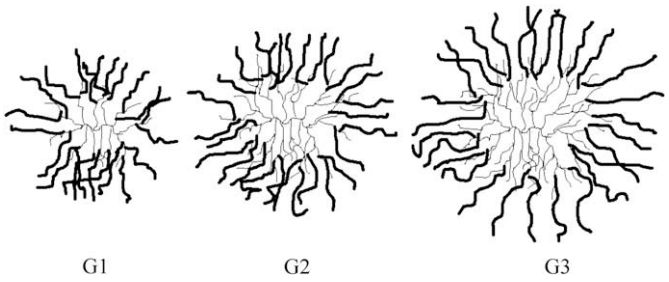

Fig. 1. Three generations of arborescent PS-*g*-P2VP copolymers.

through covalent bonding, and potentially the ability to control the release process through variations in the structure (e.g. the branching density) of the micelles.

It is clear that the polystyrene and poly(2-vinylpyridine) components of arborescent PS-*g*-P2VP copolymers are not biocompatible and that the testing conditions (0.05 M HCl solutions), necessary to solubilize the copolymers in water, are far from those typically used for controlled delivery systems. The main goal of this study was to examine the release of small molecules from arborescent copolymers as *model* highly branched micelles, to improve the understanding of the influence of branching on the release process. Fluorescence techniques were first applied to obtain information on the release of pyrene, a highly hydrophobic probe molecule, from arborescent PS-*g*-P2VP copolymers of generations *G*1–*G*3 (Fig. 1). In the second part of the investigation, the *in vitro* release of indomethacin was monitored by UV spectroscopy. The release kinetics were analyzed using the power law model and Fick's second law of diffusion. Release experiments for lidocaine from a *G*1 copolymer were also carried out to study the influence of probe structure on the release process.

2. Experimental

2.1. Materials

Pyrene (99.9%), perylene (sublimed, 99.5+%), and thallium (I) nitrate (99.9%) were purchased from Aldrich. Indomethacin (99%) and lidocaine were obtained from Sigma, while chloroform (HPLC grade) and methylene chloride (HPLC grade) were supplied by Merck. All chemicals were used as-received. Milli-Q water (18 MΩ cm) was used to prepare all sample solutions. The synthesis of the arborescent PS-*g*-P2VP copolymers used for this work was achieved [9] by grafting 'living' P2VP chains onto acetylated PS substrates of generations *G*0–*G*2. All copolymers had narrow molecular weight distributions ($M_w/M_n < 1.1$) and PS contents of at most 18% by weight.

2.2. Sample preparation

Micellar solutions were prepared by dissolving 250 mg of arborescent PS-*g*-P2VP copolymer in 50 mL of 0.05 M aqueous HCl. The micelles were loaded either with pyrene or perylene, by adding approximately 10 mg of the dyes to 5 mL of the copolymer solutions. The mixtures were stirred for three days and filtered through 0.22 μm mixed-ester membrane filters to remove solid dye residues. Loading of lidocaine and indomethacin in the copolymer was achieved by dissolving 50 mg of a drug and 50 mg of the copolymer in 1 mL of chloroform (lidocaine) or methylene chloride (indomethacin). The copolymer solutions were then precipitated in hexane. Non-encapsulated drug molecules were removed by washing the precipitates several times in hexane until no traces of the drugs were detected in the solvent with UV measurements.

2.3. Fluorescence studies

Steady-state fluorescence spectra for the pyrene/perylene FRET and pyrene quenching experiments were acquired on a Photon Technology International LS-100 spectrometer using $1.0 \times 1.0\ cm^2$ Hellma quartz cells. The slit widths on the excitation and emission monochromators were set at 2 and 1 nm, respectively. For both the energy transfer and the quenching measurements, the excitation wavelength for the emission spectra was set at 344 nm and before each measurement, a 1-pyrenemethanol standard was run to minimize inconsistencies resulting from lamp intensity variations. Time-resolved fluorescence decay curves were obtained by the time-correlated single photon counting technique using the IBH 5000U System from HORIBA Jobin Yvon Inc., with a nanosecond xenon flash lamp. The excitation wavelength used was 344 nm and the emission fluorescence decay was monitored at 372 nm. A 371 nm cut-off filter was used to prevent scattered light interference in the detector. To obtain quantitative information from the decays, the curves were fitted with a sum of exponentials using the Marquardt–Levenberg nonlinear least squares method [10]. To obtain good quality fits as estimated from the χ^2 values, the distribution and auto-correlation functions of the residuals, a sum of 4 exponentials was used. To minimize inner filter effects, the solutions for the fluorescence studies were diluted to obtain optical density values below 0.3. The FRET measurements were started immediately after mixing 1.5 mL each of the micellar solutions loaded with pyrene and perylene. The emission intensity of the acceptor (perylene) was monitored at 475 nm to minimize any contributions from the emission of the donor (pyrene). For the quenching experiments, 20–40 μL of a 0.2 M $TlNO_3$ solution were added to 3 mL of micellar solution loaded with pyrene. The fluorescence measurements were started after 10 min of equilibration.

2.4. Loading and release of indomethacin and lidocaine

A known amount of drug-loaded arborescent PS-*g*-P2VP micelles (10 mg of lidocaine- or 2 mg of indomethacin-loaded micelles) was dissolved in 10 mL of 0.05 M HCl. The amounts of drugs used in the experiments were adjusted so that the final concentrations of lidocaine and indomethacin in solution were similar. The micellar solutions were then transferred to a SPECTRA/POR® 7 dialysis bag (MWCO = 1000) and dialyzed against 100 mL of 0.05 M HCl. At predetermined time intervals 3 mL aliquots of the dialysate were removed for UV measurements. To maintain suitable sink conditions and a constant dialysate volume, 3 mL of fresh 0.05 M HCl were added to the dialysate after each withdrawal. The UV measurements were performed on a Hewlett-Packard 8452A Diode Array Spectrophotometer, after dilution of the samples to obtain absorbance readings <1.5.

3. Results and discussion

The characteristics of the arborescent PS-*g*-P2VP copolymers used in the experiments are reported in Table 1. The copolymers are based on PS cores of different generations, but all have P2VP segments of similar molecular weight ($M_w \approx 5000$). The loading capacities in Table 1 are expressed both as the number of moles of probe solubilized per gram of micelles and as the number of probe molecules per arborescent micelle. The latter values range from 6 to 530 for pyrene and from 0.5 to 21 for perylene, following the expected increasing capacity trend in the order $G1 < G2 < G3$ for both pyrene and perylene. It was shown in a recent investigation [11] that highly hydrophobic probes (such as pyrene, and likely also perylene) partition strictly into the hydrophobic core of

Table 1
Characteristics of PS-*g*-P2VP arborescent copolymers used in the study.

Overall generation	*G*1	*G*2	*G*3
M_w (g/mol)	4.7×10^5	3.7×10^6	2.2×10^7
PS weight fraction (%)	12	13	18
f_w(core)	11	84	690
f_w(copolymer)	82	630	3400
Pyrene loading			
mol/g micelles	1.32×10^{-5}	1.0×10^{-5}	2.4×10^{-5}
Molecules/micelle	6.2	37	530
Perylene loading			
mol/g micelles	1.1×10^{-6}	4.2×10^{-7}	9.6×10^{-7}
Molecules/micelle	0.52	1.6	21

f_w is the branching functionality, defined as the number of side chains added in the last grafting cycle.

arborescent micelles. Thus for the *G*1 micelles, 6 pyrene molecules are effectively dissolved in a core having a mass representing only 12% ($M_w = 5.6 \times 10^4$) of the total molecular mass ($M_w = 4.7 \times 10^5$). Considering that the copolymers investigated had low polystyrene contents (12–18% by weight), it is therefore not surprising that their hydrophobic absorption capacity is also low. The relatively small number of probe molecules solubilized per micelle likely simply reflects the low solubility of the probe molecules in polystyrene, the lower loadings attained for perylene as compared to pyrene being explained by its larger size [11].

3.1. Nonradiative energy transfer

Fluorescence resonance energy transfer (FRET) is based on a dipole–dipole coupling process allowing the transfer of energy from an excited fluorescence donor molecule to a ground state acceptor molecule without emission of a photon [12]. The rate constant for the FRET process, k_T, depends among others on the donor-to-acceptor distance r, according to the equation

$$k_T = \frac{1}{\tau_D}\left(\frac{R_0}{r}\right)^6 \quad (1)$$

where τ_D is the decay constant for the donor in the absence of the acceptor, and R_0 is the Förster radius, a parameter depending on the photophysical properties of the donor–acceptor pair including the extent of overlap of the donor emission and the acceptor absorbance spectra [13]. It also represents the distance at which the energy transfer efficiency is 50%. Time-dependent FRET measurements upon mixing two separate solutions of identical micellar concentrations, one loaded with donor molecules and the other one with acceptor molecules, have been used to characterize the release kinetics of hydrophobic probes from block copolymer micelles [14,15]. In the current study, the donor molecule selected is pyrene and the acceptor is perylene. The emission spectrum of pyrene partly overlaps with the absorption spectrum of perylene, as shown in Fig. 2 with the corresponding emission spectrum for perylene, and the pair has an R_0 value of 33.32 nm [16]. Mixing of the loaded micelles initiates the redistribution of the fluorophores among the micelles, and the time-dependent increase in the steady state perylene emission is monitored at 475 nm upon excitation of pyrene. Since the efficiency of FRET depends on diffusion, it is possible to use this method to investigate the influence of the arborescent PS-*g*-P2VP branching functionality on the probe release kinetics, as the branching functionality increases with the generation number.

The normalized experimental time-dependent fluorescence intensity ratio for perylene, R_A, used to express the FRET results shown in Fig. 3, is defined by the equation

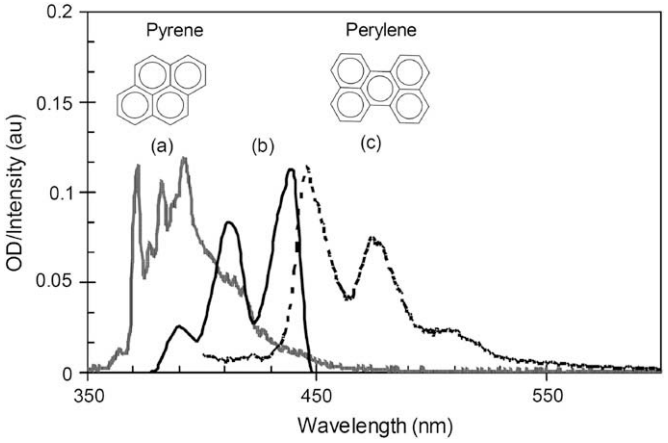

Fig. 2. Emission spectrum for pyrene excited at 344 nm (a), overlaps with absorption spectrum for perylene (b), and resulting emission spectrum for perylene (c). All spectra were recorded in toluene, and normalized to be on the same scale.

$$R_A = \frac{I_A(t) - I_A(0)}{I_A(\infty) - I_A(0)} \quad (2)$$

where $I_A(t)$ and $I_A(0)$ are the perylene emission intensities at time t at the beginning of the measurements, respectively, and $I_A(\infty)$ is the intensity at equilibrium. A rapid initial increase in R_A is observed during the first 300 min, and is followed by more gradual equilibration at longer times (Fig. 3). This corresponds to an initial burst in release followed by slow equilibration. While the overall release profile is very similar for all copolymers, there is a small influence of copolymer structure on the initial burst release.

It is seen (Fig. 3 inset) that the initial release rate is higher for the *G*1 copolymer than for the *G*2 and *G*3 molecules. This is attributed to the lower branching functionality of the *G*1 sample (Table 1). As discussed in a former investigation [11], pyrene and perylene are highly hydrophobic and should therefore be located in the PS core of the micelle. The diffusion of the probes in the core should be influenced by their branching functionality, the copolymer with a higher core branching functionality (*G*3) presumably having a lower initial release rate than the *G*2 and the *G*1 copolymers. However, the initial release rate of the *G*2 and *G*3 copolymers is essentially identical. Because of its higher PS content, sample *G*3 has a higher probe loading than sample *G*2 (Table 1). The influence of branching functionality on the initial

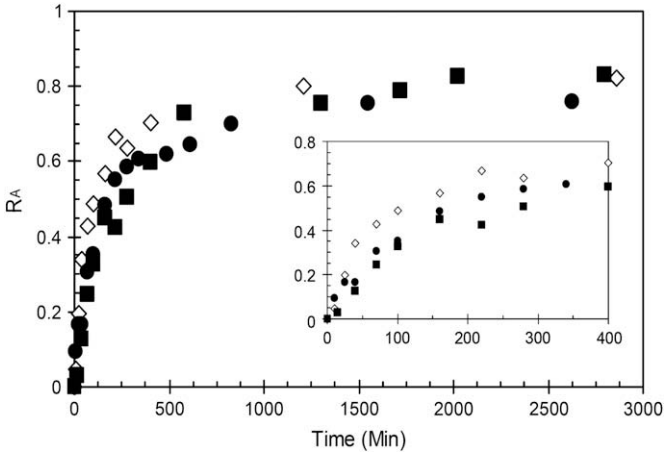

Fig. 3. Normalized perylene intensity ratios R_A for *G*1 (◇), *G*2 (■) and *G*3 (●) arborescent copolymers. The initial portion of the plot is expanded in the inset.

release rate for this sample may be counterbalanced by its higher initial probe concentration, as the flux of solute should increase with the initial concentration of the probes in the micelles.

3.2. Fluorescence quenching experiments

To clarify the influence of branching functionality on the initial release process, it is important to understand how easily small molecules can penetrate in the micelles. With fluorescence collision quenching experiments, it is possible not only to quantify the diffusion rate for small molecules but also to obtain information on the distribution of the probe molecules within the micelles [17]. In a series of quenching experiments, 20–40 μL aliquots of 0.2 M $TlNO_3$ solutions were added to a 3-mL sample of micellar solution loaded with pyrene. As an ionic quencher, thallium nitrate is expected to quench only pyrene molecules located within the P2VP shell or at the PS core–P2VP interface, since Tl^+ ions cannot penetrate inside the hydrophobic PS core [14,18]. It is therefore possible to quantify the fraction of pyrene molecules accessible to the quencher and the fraction buried within the PS core.

The kinetics of collisional fluorescence quenching in homogeneous solutions are best described by the Stern–Volmer equation,

$$\frac{I_0}{I} = 1 + k_q \tau_0 [Q] \tag{3}$$

where I_0 and τ_0 represent the unquenched fluorescence intensity and the lifetime of the fluorophore, respectively, I is the fluorescence intensity observed at a quencher concentration [Q], and k_q is the bimolecular quenching constant. The intensity of pyrene emission was determined by integration of the spectrum from 370 to 374 nm, and the number-average fluorescence lifetime $\langle\tau\rangle_0$, determined from tetraexponential fitting of the decay curves, was substituted for τ_0 in Eq. (3). A plot of I_0/I against [Q] is expected to be linear, but a plateau may be present at high quencher concentrations if protective quenching is present [17,19]. The curves in Fig. 4a clearly indicate that only a fraction of the pyrene molecules in the micelles was accessible to the ionic quencher, as the I_0/I ratio reaches a plateau at high quencher concentrations for all pyrene-loaded arborescent copolymers. Under these conditions, the data can be analyzed using the modified Stern–Volmer equation

$$\frac{I_0}{I_0 - I} = \frac{1}{f_a} + \frac{1}{f_a k_q \tau_0 [Q]} \tag{4}$$

to determine the fraction of pyrene molecules, f_a, accessible to thallium nitrate.

Table 2
Lifetimes (ns) and preexponential factors obtained from fluorescence decays.

	G1	G2	G3
τ_1 (A_1)	4.94 (0.41)	3.54 (0.64)	4.59 (0.59)
τ_2 (A_2)	23.99 (0.30)	27.87 (0.08)	28.16 (0.14)
τ_3 (A_3)	83.42 (0.22)	116.64 (0.24)	103.97 (0.20)
τ_4 (A_4)	224.59 (0.07)	184.81 (0.04)	193.81 (0.07)
$\langle\tau\rangle_0$	43.59	40.12	40.95
χ^2	1.128	1.024	1.136

To proceed with the analysis using the Stern–Volmer equations it was necessary to determine $\langle\tau\rangle_0$ from the time-resolved decay curves. All the samples exhibited multiexponential decay behavior, indicating that the pyrene molecules were located in different environments of the micelles. In all the cases, the best fit (lowest χ^2 value) was obtained with four exponentials. The lifetimes and preexponential factors obtained from the fits are listed in Table 2. Theoretically, thorough analysis of the decay profiles could provide quantitative information on each pyrene population probing a given micellar environment [19]. However, considering the complex nature of the decays possibly resulting from inherent quenching by preassociated pyrene molecules [20] and by the protonated P2VP shell [21,22], the analysis was limited to the calculation of the number-average lifetimes in the present case.

The data from Fig. 4b were combined with the $\langle\tau\rangle_0$ values in Table 2 to estimate the fraction f_a of pyrene accessible to the quencher and the bimolecular quenching constant k_q. All the curves in Fig. 4b had correlation coefficients greater than 0.99. The quenching constant k_q can be represented by the Smoluchowski equation

$$k_q = 4\pi R D N_A \tag{5}$$

where D is the sum of the diffusion coefficients for the fluorophore and the quencher, and R is the sum of the molecular radii of the fluorophore and the quencher. The value $R = 8.6$ Å was calculated from the van der Waals radii of pyrene and thallium nitrate, using the molecular modeling software Hyperchem 7.5.

The results obtained from the analysis of the quenching experiments are summarized in Table 3. The very low average fluorescence lifetime values obtained are attributed to the large fraction of species quenched by protonated P2VP chains or by other pyrene molecules. In a previous quenching study involving pyrene-labeled arborescent PS homopolymer solutions in THF, the bimolecular quenching constant was found to decrease for higher generations when nitromethane was used as quencher [23]. The

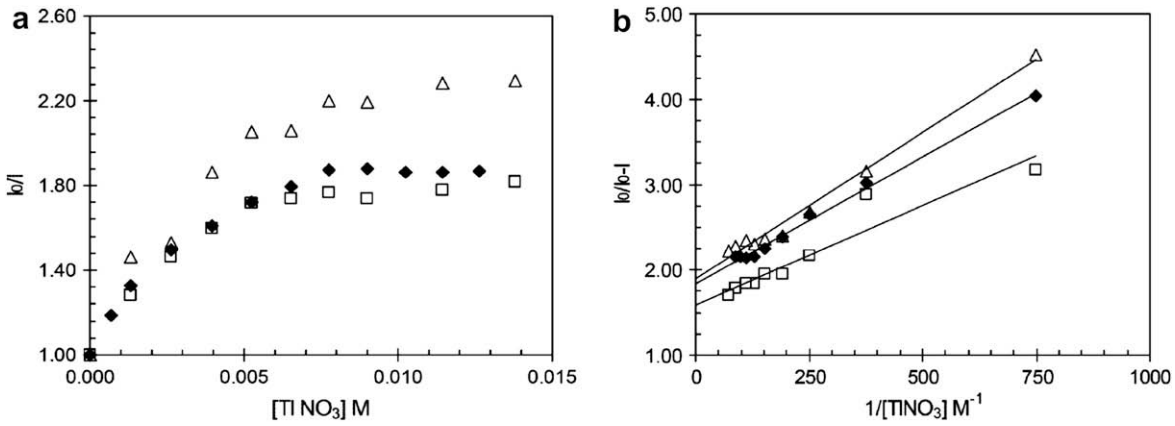

Fig. 4. (a) Stern–Volmer and (b) modified Stern–Volmer plots for pyrene-loaded *G*1 (□), *G*2 (△), and *G*3 (◆) PS-*g*-P2VP copolymers.

Table 3
Quenching data for pyrene-loaded arborescent PS-*g*-P2VP.

	f_a (%)	$\langle\tau\rangle_0$ (ns)	k_q (10^{10} M^{-1} s^{-1})	D (10^{-5} cm^2 s^{-1})
*G*0[a]	45 ± 1	53.83	0.58 ± 0.02	0.89 ± 0.03
*G*1	53 ± 2	43.59	1.27 ± 0.03	1.94 ± 0.01
*G*2	63 ± 2	40.12	2.93 ± 0.02	4.48 ± 0.02
*G*3	55 ± 1	40.95	1.48 ± 0.01	2.26 ± 0.02

[a] While the *G*0 arborescent PS-*g*-P2VP copolymers have been found to aggregate in 0.1 M HCl aqueous solutions [9], it is assumed that the microporosity of the copolymer molecules is not affected by the formation of aggregates.

quencher molecules must diffuse into the highly branched arborescent PS to encounter the pyrene molecules. Since the segmental density of arborescent polymers increases with the generation number, k_q would be expected to decrease for higher generations. In the present study, the pyrene molecules in the PS core are not polymer-bound and $TlNO_3$ is an aqueous quencher. Encounters between the quencher and probe molecules are therefore likely limited to the interfacial and the shell regions of the micelles. Consequently, the bimolecular collision constant (and hence the diffusion coefficient) should depend on the porosity of these regions. Segmental electrostatic repulsions are known to influence the structure of polyelectrolytes in solution [24,25]. For example, the hydrodynamic diameter of PS-*b*-P2VP-*b*-PEO triblock copolymer micelles in aqueous solutions was found to increase from 75 to 135 nm as the pH dropped below 5 [25]. The behavior of arborescent PS-*g*-P2VP copolymers should be likewise influenced by the polyelectrolyte character of the protonated P2VP segments in the shell.

The bimolecular quenching constant actually increases from samples *G*0–*G*2, leading to an increase in diffusion coefficient D, as it is directly related to k_q through Eq. (5). This trend is opposite to the results obtained for nitrobenzene quenching of (neutral) pyrene-labeled arborescent polystyrenes [23]. The increase in k_q and D observed from the generations *G*0–*G*2 copolymers is attributed to the large number of protonated P2VP segments increasing the electrostatic repulsions in the copolymer molecules. The increase in D from 0.89×10^{-8} cm^2 s^{-1} for the *G*0 or comb-branched copolymer ($f_w = 12$) to $D = 4.48 \times 10^{8}$ cm^2 s^{-1} for the *G*2 copolymers ($f_w = 690$) is consistent with increased electrostatic repulsions in the interfacial and P2VP shell regions facilitating the penetration of quencher molecules into the micelles. For the same reason, it is not surprising that the fraction of pyrene molecules accessible to thallium nitrate (f_a) increases from *G*0 to *G*2. The k_q and D values determined for the *G*3 copolymer sample are unexpectedly low. While the cause of this deviation is not very clear, it could be due to the dominating influence of the high branching functionality of the copolymer ($f_w = 3400$) on its structural rigidity.

It would have been interesting to analyze the time-dependent energy transfer curves using known release kinetic models, however the complex nature of the FRET process renders such an analysis extremely difficult [15]. The distribution of fluorophores among micelles is a multi-step process that comprises the release from one set of micelles, diffusion through the aqueous medium, and uptake by the other micelles. Furthermore, there is difficulty in relating fluorescence intensities to the amount of probe released because the pyrene fluorescence is quenched by preassociated species, and both probes can be quenched by protonated P2VP chains [26]. To avoid these problems, indomethacin was selected to study the release kinetics from arborescent PS-*g*-P2VP copolymers by dialysis, for comparison with the results obtained in the fluorescence studies. Release studies for lidocaine were also performed with the *G*1 copolymers, to study the influence of probe structure on the release process.

3.3. In vitro *release kinetics of indomethacin and lidocaine*

Indomethacin and lidocaine were selected as model drugs for the release experiments on the basis of their ready availability and of the large body of literature available on that topic. Total drug loading was determined by dissolving the loaded micelles in ethanol and measuring the UV absorption of the solution at $\lambda_{max} = 232$ nm for indomethacin and $\lambda_{max} = 262$ nm for lidocaine. Loadings of 46, 42, and 43% indomethacin by weight were obtained for the *G*1–*G*3 copolymers, respectively. For lidocaine, a loading of 8% by weight was obtained for the *G*1 copolymer. The low encapsulation efficiency observed for lidocaine (Fig. 5b) is presumably due to its high solubility in hexane and weak interactions with the micelles. In contrast, indomethacin (Fig. 5a) is sparingly soluble in hexane and is expected to interact strongly with the P2VP segments of the micelles. The encapsulation efficiency has indeed been found to increase with decreasing solubility of the small molecules in the recovery medium [27,28].

The release profiles obtained in 0.05 M HCl for indomethacin- and lidocaine-loaded *G*1 arborescent PS-*g*-P2VP copolymers are compared in Fig. 6. In contrast to the rapid release observed for the free probes from dialysis tubing (100% release in less than 5 h), the release from the dendritic micelles is slow, corresponding to sustained characteristics. Each release experiment was performed twice. Values of *t* tests obtained from the release data did not show any statistical difference between the results at a confidence level of 95%. For both indomethacin and lidocaine, an initial burst in release is observed for the first 5 h but is followed by more gradual release until equilibration is attained over 1–2 days. Furthermore, while roughly 80% of the loaded lidocaine is released at equilibrium, only about 40% of the indomethacin is released from the micelles (Fig. 7). Lidocaine is less hydrophobic (Log $P = 2.4 \pm 0.3$), a large fraction of the probe is presumably located in the unprotonated P2VP shell after encapsulation. This fraction is completely released within the time frame of the release experiment.

The incomplete release of indomethacin from the micelles cannot be attributed simply to reservoir (dialysate) saturation, as a similar mass fraction versus time profile was obtained in a preliminary experiment with a doubled dialysate volume. The incomplete release is more likely related to physical entrapment of the drug in the hydrophobic core and/or the palisade (interfacial) regions of the micelles, due to the moderately hydrophobic character (Log $P = 3.1 \pm 0.4$) of indomethacin. A similar explanation was suggested for the incomplete release of indomethacin from block copolymer micelles incorporating a hydrophobic poly(ε-caprolactone) core and a hydrophilic poly(ethylene glycol) shell [29]. Another possibility could be hydrogen bonding interactions between the pyridine ring of P2VP chain segments and the carboxylate group of indomethacin. The formation of hydrogen bonds between indomethacin and poly(vinyl pyrrolidone) units has been reported [30,31], and determined to involve the carboxylic acid group of indomethacin and the carbonyl group of the pyrrole ring. The lack of hydrogen bond formation with the nitrogen atom in the pyrrole ring was attributed to steric hindrance. In the PS-*g*-P2VP micelles, nitrogen in the pyridine ring is not sterically hindered and should be capable of forming hydrogen bonds, since

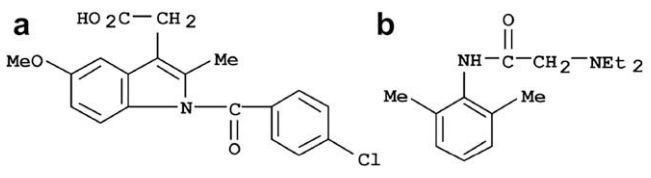

Fig. 5. Structures of indomethacin (a) and lidocaine (b).

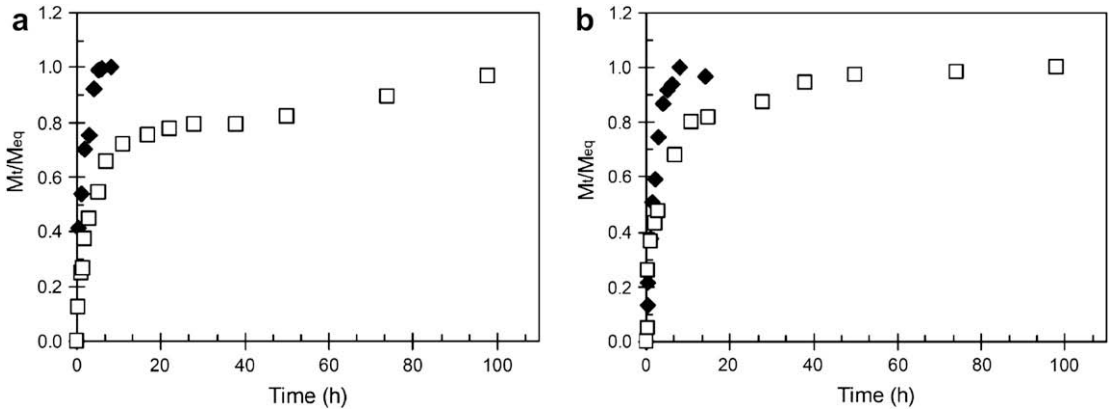

Fig. 6. Release profile for (a) indomethacin and (b) lidocaine in 0.05 M HCl in the free state (◆) and from *G*1 PS-*g*-P2VP copolymer (□). M_t is the cumulative weight released at time t, and M_{eq} is at equilibrium.

indomethacin was loaded in the micelles before dissolution in the HCl solution. There are no strong interactions between lidocaine and the micelles, which would likewise explain why a larger fraction of the encapsulated drug was released.

The influence of the micelle generation number on the release of indomethacin (Fig. 7) is similar to that observed in the FRET studies using the fluorescent probes. The release profile for the *G*1 micelles shows an initial burst in release, which decreases in magnitude for higher generations, the *G*3 copolymer having a more linear profile. While the *G*1–*G*3 copolymers had comparable micellar loadings, the amount of probe released at equilibrium decreased for higher generations. At equilibrium more than 40% of the indomethacin loaded in the *G*1 micelles was released (Fig. 7), while about 30% and less than 20% were released from the *G*2 and *G*3 samples, respectively. This result suggests that the number of probe molecules encapsulated in the highly branched glassy PS core/palisade regions of the micelles increases with the size of the micelles, and therefore the fraction of drug molecules release within the time frame of the experiment decreases.

The influence of indomethacin loading (controlled by varying the weight fraction of copolymer and drug during encapsulation) on the release process for *G*1 micelles is illustrated in Fig. 8. The initial release rate and the mass fraction of indomethacin released at equilibrium both increase with loading. For loadings of 29, 33, and 46% w/w, for instance, the fraction of indomethacin released from the *G*1 arborescent PS-*g*-P2VP copolymers after 20 h was 18, 30, and 33%, respectively. The dependence of the indomethacin release on its concentration in the micelles is consistent with a diffusion-controlled release mechanism. As the concentration of indomethacin in the micelles is increased the fraction of molecules in the P2VP shell presumably increases, leading to faster release of the probe.

The release data were analyzed using a power law model [32], the semi-empirical equation

$$\frac{M_t}{M_{eq}} = kt^n \tag{6}$$

formerly used to describe the release from polymeric systems for up to 55% of the equilibration level [33]. In the power law model, k is a constant dependent upon the structural and geometric characteristics of the device. Its magnitude is usually indicative of solvent–solute or device–solute interactions, high values reflecting strong solvent–solute or weak device–solute interactions. The release exponent n depends on the release mechanism, $n = 1.0$ representing a release rate independent of time or zeroth-order release kinetics. This type of release mechanism is also known as case-II transport and typically involves time-dependent swelling of the delivery device. A value of $n < 0.43$ is indicative of Fickian

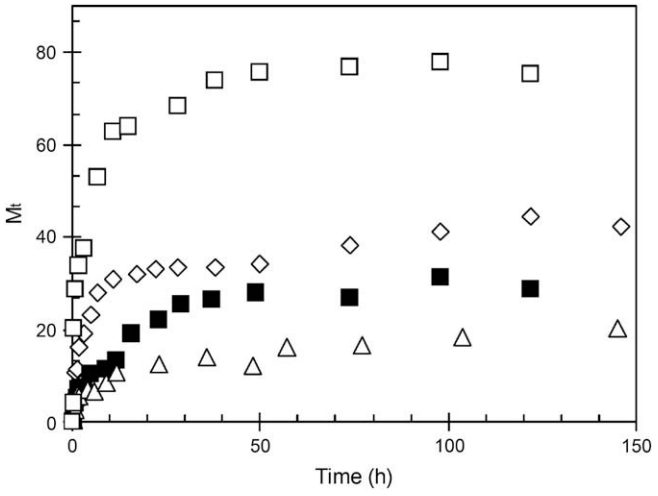

Fig. 7. Percentage mass fraction of indomethacin released from *G*1 (◇), *G*2 (■), and *G*3 (△) copolymers, and lidocaine released from the *G*1 (□) copolymer.

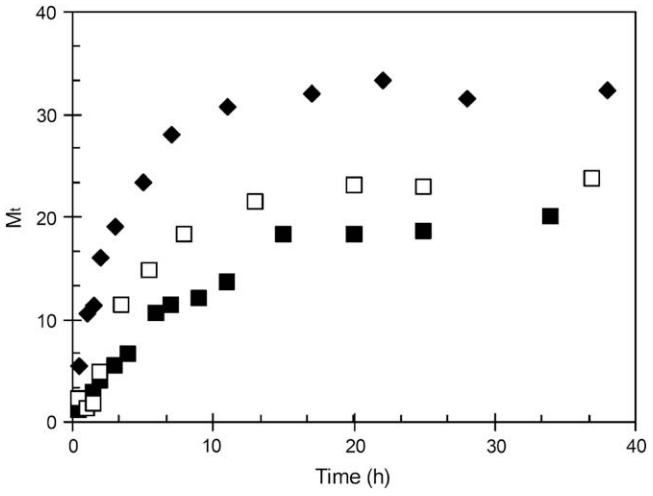

Fig. 8. Influence of initial indomethacin loading (w/w) on release from *G*1 micelles: 29% loading (■); 33% loading (□); 46% loading (◆).

Table 4
Parameters k and n of the power law model for the release of indomethacin from PS-*g*-P2VP copolymers.

	*G*1	*G*2	*G*3
n	0.60 ± 0.04	0.48 ± 0.01	0.39 ± 0.06
k	0.21 ± 0.03	0.14 ± 0.02	0.15 ± 0.04

diffusion control of the release process. Intermediate n values (0.43–1.0), corresponding to anomalous transport, may be regarded as a combination of both mechanisms. The values of n quoted here are only valid for release devices with a spherical geometry, and actually vary with the shape of the device.

Experimental values of k and n were determined for the PS-*g*-P2VP micelles by the linear least squares method. It can be seen from Table 4 that for approximately 40% loading, the release mechanism for indomethacin changes from anomalous transport to Fickian (diffusion-controlled) as the generation number of the arborescent PS-*g*-P2VP copolymers increases. No clear trend can be observed among the k values, although the *G*1 copolymers had a significantly higher value suggesting the most favorable interactions between the probe and solvent. For comparison lidocaine, which is more soluble in 0.05 M HCl, had $n = 0.34$ and $k = 0.34$ in the *G*1 micelles.

Considering that the release of indomethacin from arborescent PS-*g*-P2VP copolymers is apparently dominated by diffusion, Fick's second law of diffusion was used to estimate the diffusion coefficient of indomethacin in the micelles and the initial burst release rate from the micelles to their immediate surroundings (i.e. 0.05 M HCl). The amount of material diffusing out of a homogeneous sphere at time t can be calculated from the exact solution to Fick's second law of diffusion given by [34]

$$\frac{M_t}{M_\infty} = 1 - \frac{6}{\pi^2}\sum_{n=1}^{\infty}\frac{1}{n^2}\exp\left(-Dn^2\pi^2 t/r^2\right) \tag{7}$$

where D is the average diffusion coefficient of the substance within the sphere, n is the number of iterations used for the calculations, and r is the radius of the sphere. To calculate the initial burst release rate, the early time approximation of Eq. (7) [35]

$$\frac{M_t}{M_\infty} = 6\left(\frac{D_i t}{r^2\pi}\right)^{1/2} - \frac{3D_i t}{r^2} \tag{8}$$

can be derived with respect to time to give the early time release rate

$$\frac{d(M_t/M_\infty)}{dt} = 3\left(\frac{D_i}{r^2\pi t}\right)^{1/2} - \frac{3D_i}{r^2}. \tag{9}$$

Eqs. (8) and (9) are typically valid over the first 40% of the release process. The early time diffusion coefficient (D_i), the average diffusion coefficient (D), and the early time release rate were determined by fitting Eqs. (7)–(9), respectively, to the experimental data and by minimizing the χ^2 value obtained using Mathcad 2000 Professional software.

The diffusion coefficients for indomethacin in arborescent PS-*g*-P2VP copolymers (Table 5) are much lower than those reported in the literature for the same probe in other controlled release devices. For example, $D \approx 3.5 \times 10^{-10}$ cm^2 s^{-1} was reported for pressure sensitive-adhesive devices made from polystyrene-*block*-polyisoprene copolymers [36], and $D \approx 2.7 \times 10^{-16}$ cm^2 s^{-1} was reported for poly(L-lactic acid)-*block*-poly(ethylene glycol) micelles [4]. The low D values obtained herein, on the order of 10^{-18} cm^2 s^{-1}, could be related to the highly branched structure of the arborescent copolymers.

Table 5
Diffusion coefficients of indomethacin in arborescent PS-*g*-P2VP copolymers.

	*G*1	*G*2	*G*3
Radius[a] (nm)	12.5	22.5	39.5
D_i[b] (cm^2 s^{-1})	2.54×10^{-18} (0.03)	2.81×10^{-18} (0.01)	7.08×10^{-18} (0.13)
Average D[c] (cm^2 s^{-1})	1.25×10^{-18} (0.18)	4.67×10^{-18} (0.07)	4.33×10^{-18} (0.08)
Rate[d] (s^{-1}) at 2 h	2.06×10^{-5}	1.31×10^{-5}	1.19×10^{-5}

[a] Determined from dynamic light scattering measurements.
[b] Early time diffusion coefficient obtained from Eq. (8).
[c] Obtained by fitting Eq. (7) to experimental data.
[d] Initial release rate obtained from Eq. (9). The values within parentheses are the χ^2 parameters for the fits.

The trend among the diffusion coefficients D for indomethacin in Table 5 is consistent with that determined for pyrene (Table 3). While a decrease in the diffusion coefficient might have been expected for higher generation copolymers due to their increased branching functionality, D_i generally increases. This is again attributed to the increased electrostatic repulsions between P2VP segments for higher generation copolymers upon protonation, as discussed earlier. After dissolution in dilute HCl, protonation leads to electrostatic repulsions causing the P2VP chains to stretch, and to an increase in the volume of the hydrophilic shell [9,24,25]. While the resulting volume expansion tends to be less significant for higher generation arborescent PS-*g*-P2VP copolymers [24], it appears that the electrostatic repulsions still suffice to increase the microporosity and the diffusion coefficients for the micelles. The lower D value obtained for the *G*3 copolymer, though not very significant, is again consistent with increased structural rigidity for the *G*3 molecules as discussed earlier. In contrast, the initial diffusion coefficient D_i increases continuously from *G*1 to *G*3 copolymers, presumably because the indomethacin molecules diffuse predominantly out of the corona initially. While D_i increases with the generation number, the initial release rate decreases (Table 5). Theses two trends may sound contradictory, but they simply arise because the initial release rate varies inversely with the radius of a sphere (Eq. (9)), and the size of arborescent PS-*g*-P2VP copolymer micelles increases with the generation number (Table 5).

4. Conclusions

The release of small molecules from arborescent copolymer micelles incorporating a branched polystyrene core and poly(2-vinylpyridine) segments in the shell was investigated. The release profiles obtained display sustained release characteristics with an initial burst, followed by slow approach to equilibrium. The diffusion coefficients for pyrene determined from fluorescence quenching experiments, and the average diffusion coefficients for indomethacin estimated by fitting an exact solution of Fick's second law of diffusion for a spherical device to the experimental data displayed the same increasing trend from *G*1 to *G*2, while a decrease was observed for the *G*3 micelles. In spite of the increasing branching functionality of the copolymer micelles with the generation number, the results obtained from the fluorescence and the *in vitro* release studies are consistent with a more porous microstructure in acidified media for higher generation arborescent PS-*g*-P2VP copolymers up to *G*2. The increased number of P2VP chains per micelle for higher generation micelles presumably leads to enhanced electrostatic repulsions between the charged P2VP chains of higher generation arborescent PS-*g*-P2VP copolymers. Despite increased electrostatic repulsions, the average diffusion coefficient decreased for the *G*3 copolymers, hinting at the dominating influence of branching functionality (branching density) on the structural rigidity of the molecules.

Acknowledgements

The financial support of the Natural Sciences and Engineering Research Council of Canada (NSERC) and the International Council for Canadian Studies (ICCS) is acknowledged with thanks. We also thank Prof. Jean Duhamel (Department of Chemistry, University of Waterloo) for providing access to the fluorescence characterization equipment.

References

[1] Kwon G, Naito M, Yokoyama M, Okano T, Sakurai Y, Kataoka K. J Controlled Release 1997;48:195–201.
[2] Webber SE. J Phys Chem B 1998;102:2618–26.
[3] Teng Y, Morrison ME, Munk P, Webber SE, Procházka K. Macromolecules 1998;31:3578–87.
[4] Kim SY, Kim JH, Kim D, An JH, Lee DS, Kim SC. J Appl Polym Sci 2001;82:2599–605.
[5] Shen E, Kipper MJ, Dziadul B, Lim M-K, Narasimhan B. J Controlled Release 2002;82:115–25.
[6] For applications of dendrimers in drug release, see for example:
(a) Patri AK, Kukowska-Latallo JF, Baker Jr JR. Adv Drug Delivery Rev 2005;57:2203–14;
(b) Tomalia DA, Reyna LA, Svenson S. Biochem Soc Trans 2007;35:61–7.
[7] For applications of hyperbranched polymers in drug release, see for example:
(a) Tuerk H, Shukla A, Rodrigues PCA, Rehage H, Haag R. Chem A Eur J 2007;13:4187–96;
(b) Zhang JG, Krajden OB, Kainthan RK, Kizhakkedathu JN, Constantinescu I, Brooks DE, et al. Bioconjugate Chem 2008;19:1241–7;
(c) Liu H, Chen Y, Zhu D, Shen Z, Stiriba S-E. React Funct Polym 2007;67:383–95.
[8] Liu M, Kono K, Fréchet JMJ. J Controlled Release 2000;65:121–31.
[9] Gauthier M, Li J, Dockendorff J. Macromolecules 2003;36:2642–8.
[10] Press WH, Teukolsky SA, Wetterling WT, Flannery BP. Numerical recipes in C: the art of scientific computing. Cambridge: Cambridge University; 1992. p. 683.
[11] Njikang G, Gauthier M, Li J. Polymer 2008;49:1276–84.
[12] Masuko M, Ohuchi S, Sode K, Ohtani H, Shimadzu A. Nucleic Acids Res 2000;28:e34.
[13] Lakowicz JR. Principles of fluorescence spectroscopy. New York: Kluwer Academic/Plenum; 1999. p. 367.
[14] Cao T, Munk P, Ramireddy C, Tuzar Z, Webber SE. Macromolecules 1991;24:6300–5.
[15] Štěpánek M, Krijtová K, Limpouchová Z, Procházka K, Teng Y, Munk P, et al. Acta Polym 1998;49:103–7.
[16] Berlman IB. Energy transfer parameters of aromatic compounds. New York: Academic; 1973. p. 358.
[17] Lakowicz JR. Principles of fluorescence spectroscopy. New York: Kluwer Academic/Plenum; 1999 [chapter 8].
[18] Bromberg L, Magner E. Langmuir 1999;15:6792–8.
[19] Claracq J, Santos SFCR, Duhamel J, Dumouseaux C, Corpart J-M. Langmuir 2002;18:3829–35.
[20] Ḥrdlovič P, Lukáč I. J Photochem Photobiol A Chem 2000;133:73–82.
[21] Štěpánek M, Krijtová K, Procházka K, Teng Y, Webber SE, Munk P. Acta Polym 1998;49:96–102.
[22] Clements JH, Webber SE. Macromolecules 2004;37:1531–6.
[23] Frank RS, Merkle G, Gauthier M. Macromolecules 1997;30:5397–402.
[24] Kee RA, Gauthier M. Macromolecules 2002;35:6526–32.
[25] Sauer M, Meier W. Colloidal nanoreactors and nanocontainers. In: Caruso F, editor. Colloids and colloid assemblies. Weinheim: Wiley-VCH; 2004. p. 160.
[26] Clements JH, Webber SE. J Phys Chem B 1999;103:9366–77.
[27] Kumbar SG, Kulkarni AR, Dave AM, Aminabhavi TM. J Hazard Mater 2002;89:233–9.
[28] Kumbar SG, Dave AM, Aminabhavi TM. J Appl Polym Sci 2003;90:451–7.
[29] Kim SY, Shin IG, Lee YM, Cho CS, Sung YK. J Controlled Release 1998;51:13–22.
[30] Taylor LS, Zografi G. Pharm Res 1997;14:1691–8.
[31] Forster A, Hempenstall J, Rades T. Internet J Vib Spectrosc 2001;5(2):6.
[32] Siepmann J, Peppas NA. Adv Drug Delivery Rev 2001;48:139–57.
[33] Aminabhavi TM, Harlapur SF, Balundgi RH, Ortego JD. J Appl Polym Sci 1996;59:1857–70.
[34] Crank J. The mathematics of diffusion. Oxford: Clarendon; 1975. p. 91.
[35] Baker RW, Lonsdale HK. Controlled release: mechanisms and rate. In: Tanquary AC, Lacey RE, editors. Controlled release of biologically active agents. New York: Plenum; 1974. p. 46.
[36] Hayashi T, Yamazaki T, Yamaguchi Y, Sugibayashi K, Morimoto Y. J Controlled Release 1997;43:213–21.